Computer Simulation of Transient Processes in a 25 kV AC Traction Network

Abdulaziz Rakhmonberdiev[1] and Alexander Manakov[2]
[1]*Department of Automation and Remote Control, Tashkent State Transport University, Temiryolchilar Str. 1, 100167 Tashkent, Uzbekistan*
[2]*Emperor Alexander I St. Petersburg State Transport University, Moskovsky Ave. 9, 190031 Saint Petersburg, Russia*
raa19860102@gmail.com, manakoff_2@mail.ru

Keywords: AC Traction Network, Short Circuit, Emergency Processes, Transient Process, Hazardous Electromagnetic Influences (HEMI), Track Circuit (TC), Mathematical Model, State Variable Method.

Abstract: This paper proposes a distributed-parameter mathematical model of a 25 kV AC traction power network developed using the state variable method for the analysis of HEMI affecting railway TC equipment. The model is formulated on the basis of an equivalent circuit representation and a loop-branch topological matrix, resulting in a system of algebraic and differential equations in state variable method. Transient voltages and currents during contact wire-to-rail short-circuit events are investigated for different fault locations and rail-to-ground resistance values corresponding to summer and winter operating conditions. Simulation results show a significant dependence of current distribution and rail-to-ground overvoltages on environmental parameters. Under winter conditions, the rail-to-ground voltage exceeds permissible insulation levels for TC, indicating the necessity of dedicated protective measures. To simplify the assessment of electromagnetic impact, an equivalent representation using generalized resistance and inductance parameters for each half-wave of the short-circuit current is introduced. The proposed model is validated by comparison with field experimental data from a 25 kV AC traction network, demonstrating an error below 8%.

1 INTRODUCTION

Electrified railways with 25 kV AC traction power supply systems generate significant HEMI that affects railway automation and TC equipment. During contact wire–to–rail short circuits, high transient currents and overvoltages arise in the return traction network and reach signaling devices through conductive and inductive coupling, which may damage insulation and disrupt safety-critical systems. Existing studies mainly use lumped or steady-state models, which are insufficient for accurate transient analysis of distributed traction networks. Therefore, this study develops a distributed-parameter mathematical model of a 25 kV AC traction network using the state variable method. The model is based on an equivalent circuit and a loop-branch topological matrix, allowing transient voltages and currents to be analyzed for different fault locations and rail-to-ground resistance conditions.

For practical evaluation of HEMI impact on TC, an equivalent representation with generalized resistance and inductance parameters for each half-wave of the short-circuit current is proposed. The model is validated by field data from an operating traction network and can be used to design coordinated protection measures for railway automation equipment.

Compared with the earlier equivalent-circuit approach reported in [1], the present study extends the analysis by introducing a distributed-parameter state-variable model, explicitly accounting for seasonal rail-to-ground resistance variations, deriving equivalent half-wave parameters, and validating the results against field experimental data.

2 MATHEMATICAL MODEL OF A 25 KV AC TRACTION NETWORK

The equivalent circuit diagram of an AC traction network with distributed parameters is shown in Figure 1, where: U_{TS} is the voltage on the traction transformer (TT); R_E is the resistance of the TT windings; L_E is the TT inductance; $R_{(r\text{-}G)1}$, …, $R_{(r\text{-}G)N}$ is the resistance of 1 km of the rail line section between the rails and the ground (rail-to-ground resistance); where N is the number of sections with a length of 1 km; R_0 is the resistance between the ground and the rails at the connection point of the suction feeder of the TS; R_{G1}, …, R_{GN} are the resistances of 1 km of the ground; R_{K1}, …, R_{KN} is the resistance of 1 km of the catenary; L_{K1}, …, L_{KN} is the inductance of 1 km of the catenary; R_{r1}, …, R_{rN} is the resistance of 1 km of the rails; L_{r1}, …, L_{rN} is the inductance of 1 km of the rails; C is the capacitance of the shunt compensation system capacitors; L is the inductance of the shunt compensation system reactor; R_{Ir1}, …, R_{IrN} is the 1-km insulation resistance between the overhead contact system and the rails; R_L is the resistance determined using the state variable method.

The state variable method was applied to analyze HEMI produced by the 25 kV AC traction network on TC equipment. Within this framework, voltages across inductive components and currents through capacitive components, as well as voltages and currents of resistive circuit elements y(t), are expressed as functions of the state vector x(t) and the independent excitation sources u(t).

The vectors of voltages and currents of nonreactive elements y(t), together with the inductor voltages and capacitor currents at the initial time instant, are obtained from relations (1) and (2). This requires the prior specification of both the independent sources u(t) and the initial values of the state variables x(t) [1]-[7]:

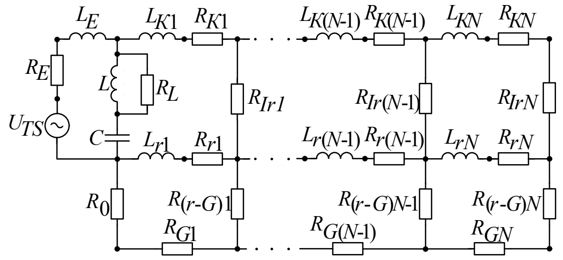

Figure 1: Equivalent circuit diagram of an AC traction network with distributed parameters.

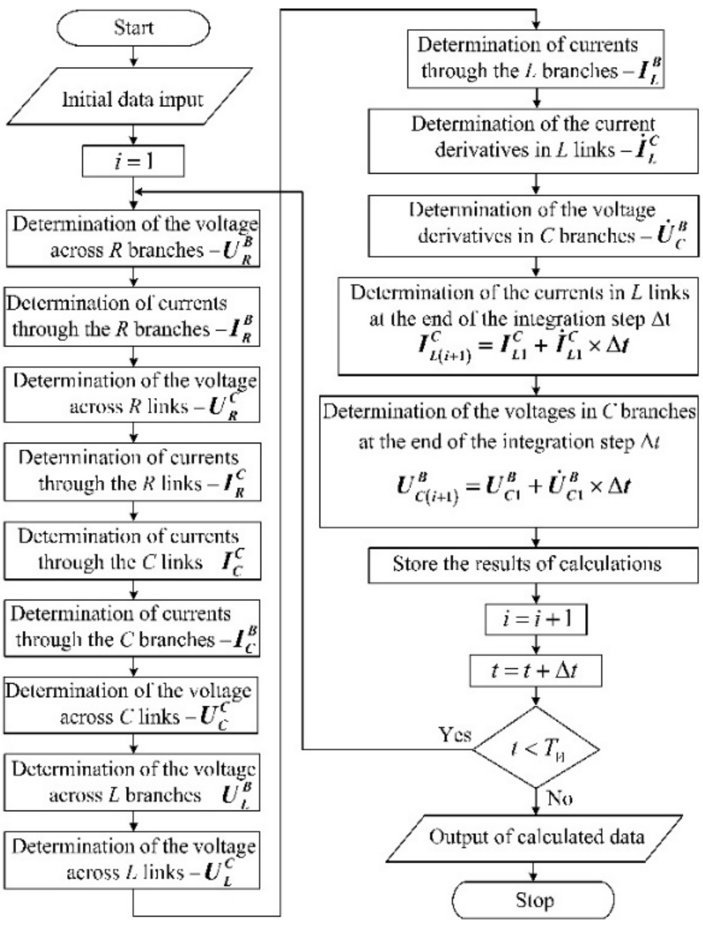

Figure 2: Algorithm of the program for calculating currents and voltages during a short circuit in the traction network.

$$\dot{x}(t) = f_1[x(t), u(t)], \quad (1)$$

$$y(t) = f_2[x(t), u(t)]. \quad (2)$$

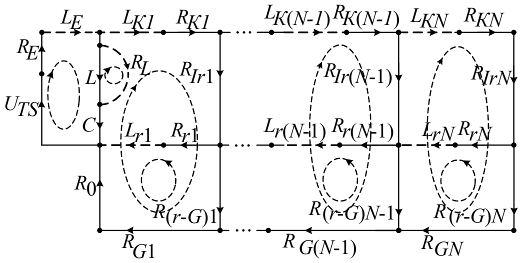

Figure 3: Tree of the linear directed graph of the equivalent circuit of the 25 kV AC traction network shown in Figure 1.

Equation (1) is numerically integrated to compute the state vector x(t) at the end of each integration interval. The resulting state vector is then used as the initial condition for the subsequent step. This iterative procedure is repeated for a predetermined number of steps (see Fig. 2).

The state variable method employs first-order differential equations. The number of differential equations corresponds to the number of reactive components in the circuit. According to the requirements of the state variable method, a linear directed graph was constructed for the equivalent circuit of the 25 kV AC traction network. Based on this linear directed graph, a directed-graph tree of the circuit was then formed (Fig. 3).

In Figure 3, arrows indicate the directions of currents in all components of the circuit. Solid lines represent the branches of the linear directed-graph tree, while dashed lines indicate the connections of the tree. Loops with positive current traversal in closed circuits are marked with dashed circles.

Using the tree of the linear directed graph, the topological F-matrix was constructed (Fig. 4). The principle of forming the F-matrix is presented in [2].

Using this matrix, Kirchhoff's laws were formulated in matrix form as:

$$U^C(t) = -F \times U^B(t), \quad (3)$$

$$I^B(t) = F^T \times I^C(t), \quad (4)$$

Where:

- F^T – denotes the transpose of the F-matrix;
- $U^B(t)$ and $I^B(t)$ – are the vectors of branch voltages and currents of the linear directed graph;
- $U^C(t)$, $I^C(t)$ – are the vectors of link (chord) voltages and currents of the linear directed graph.

By means of the *F*-matrix, coupled systems of algebraic and differential equations were formulated in the Cauchy (state variable method) form [2].

The voltages across the branch resistances U_R^B are given by:

$$\begin{cases} U_{RE} = R_E \times I_{LE}; \\ U_{RL} = R_L \times (I_{LE} - I_L - I_{LK1}); \\ U_{RK1} = R_{K1} \times I_{LK1}; \\ \vdots \\ U_{RKN} = R_{KN} \times I_{LKN}; \\ U_{Rr1} = R_{r1} \times I_{Lr1}; \\ \vdots \\ U_{RrN} = R_{rN} \times I_{LrN}; \\ U_{RG1} = R_{G1} \times (I_{LK1} - I_{Lr1}) \\ \vdots \\ U_{RGN} = R_{G1} \times (I_{LKN} - I_{LrN}); \\ U_{R0} = R_0 \times (I_{LK1} - I_{Lr1}); \\ U_{R(r-G)1} = R_{(r-G)1} \times (I_{LK1} - I_{LK2} - I_{Lr1} + I_{Lr2}); \\ \vdots \\ U_{R(r-G)N} = R_{(r-G)N} \times (I_{LKN} - I_{LrN}); \\ U_{RIr1} = R_{Ir1} \times (I_{LK1} - I_{LK2}); \\ \vdots \\ U_{RIrN} = R_{IrN} \times I_{LKN}. \end{cases} \quad (5)$$

BRANCHES

LINKS	U_{TS}	C	R_E	R_L	R_{K1}	…	$R_{K(N-1)}$	R_{KN}	R_{r1}	…	$R_{r(N-1)}$	R_{rN}	R_{G1}	…	$R_{G(N-1)}$	R_{GN}	R_0	$R_{(r-G)1}$	…	$R_{(r-G)N-1}$	$R_{(r-G)N}$	R_{Ir1}	…	$R_{Ir(N-1)}$	R_{IrN}
L_E	1	1	1	1																					
L				-1																					
L_{K1}		-1		-1	1								1				1	1				1			
⋮						⋱								⋱					⋱				⋱		
$L_{K(N-1)}$							1								1				⋱	1				1	
L_{KN}								1								1				-1	1			-1	1
L_{r1}									1				-1				-1	-1							
⋮										⋱				⋱					⋱						
$L_{r(N-1)}$											1				-1					-1					
L_{rN}												1				-1				1	-1				

Figure 4: Topological F-matrix of the tree of the linear directed graph shown in Figure 3.

The currents through the branch resistances I_R^B are defined as:

$$\begin{cases} I_{RE} = I_{LE}; \\ I_{RL} = I_{LE} - I_L - I_{LK1}; \\ I_{RK1} = I_{LK1}; \\ \vdots \\ I_{RKN} = I_{LKN}; \\ I_{Rr1} = I_{Lr1}; \\ \vdots \\ I_{RrN} = I_{LrN}; \\ I_{RG1} = I_{LK1} - I_{Lr1}; \\ \vdots \\ I_{RGN} = I_{LKN} - I_{LrN}; \\ I_{R0} = I_{LK1} - I_{Lr1}; \\ I_{R(r-G)1} = I_{LK1} - I_{LK2} - I_{Lr1} + I_{Lr2}; \\ \vdots \\ I_{R(r-G)N} = I_{LKN} - I_{LrN}; \\ I_{RIr1} = I_{LK1} - I_{Lr1}; \\ \vdots \\ I_{RIrN} = I_{LKN}. \end{cases} \quad (6)$$

The current through the branch capacitance I_C^B is defined as:

$$I_C = I_{LE} - I_{LK1}. \quad (7)$$

The voltages across the link inductances U_L^L are expressed as:

$$\begin{cases} U_{LE} = -U_{TS} - U_C - U_{RE} + U_{RL}; \\ U_L = U_{RL}; \\ U_{LK1} = U_C + U_{RL} - U_{RK1} - U_{R0} - U_{RG1} - U_{RIr1}; \\ U_{LK2} = -U_{RK2} + U_{R(r-G)1} - U_{R(r-G)2} - \\ \quad -U_{RG2} + U_{RIr1} - U_{RIr2}; \\ \vdots \\ U_{LKN} = -U_{RKN} + U_{R(r-G)N-1} - U_{R(r-G)N} - \end{cases} \quad (8)$$

$$\begin{cases} -U_{RgN} + U_{RIr(N-1)} - U_{RIrN}; \\ U_{LP1} = -U_{Rr1} + U_{R0} - U_{R(r-G)1} + U_{RG1}; \\ \vdots \\ U_{LPN} = -U_{RrN} - U_{R(r-G)N-1} + U_{R(r-G)N} + U_{RGN}; \end{cases}$$

The time derivative of the branch capacitor voltage is given by dU_C^B/dt:

$$\dot{U}_C = I_C/C; \quad (9)$$

The time derivatives of the currents through the link inductances are expressed as dI_L^L/dt:

$$\begin{cases} \dot{I}_{LE} = U_{LE}/L_E; \\ \dot{I}_L = U_L/L; \\ \dot{I}_{LK1} = U_{LK1}/L_{K1}; \\ \vdots \\ \dot{I}_{LKN} = U_{LKN}/L_{KN}; \\ \dot{I}_{Lr1} = U_{Lr1}/L_{r1}; \\ \vdots \\ \dot{I}_{LrN} = U_{LrN}/L_{rN}; \end{cases} \quad (10)$$

The voltage across the branch capacitance at the end of the integration step is determined as U_C^B:

$$U_C = U_C + \dot{U}_C \times dt. \quad (11)$$

The currents through the link inductances at the end of the integration step are obtained as I_L^L:

$$\begin{cases} I_{LE} = I_{LE} + \dot{I}_{LE} \times dt; \\ I_L = I_L + \dot{I}_L \times dt; \\ I_{LK1} = I_{LK1} + \dot{I}_{LK1} \times dt; \\ \vdots \\ I_{LKN} = I_{LKN} + \dot{I}_{LKN} \times dt; \\ I_{Lr1} = I_{Lr1} + \dot{I}_{Lr1} \times dt; \\ \vdots \\ I_{LrN} = I_{LrN} + \dot{I}_{LrN} \times dt; \end{cases} \quad (12)$$

The state variable method enables the evaluation of currents in all elements of the equivalent circuit and voltages across all components during transient regimes, including configurations involving nonlinear voltage-current characteristics.

The differential equations were solved using the simple Euler numerical integration method.

3 COMPUTER SIMULATION OF TRANSIENT PROCESSES IN A 25 kV AC TRACTION NETWORK

To solve the system of equations (5)…(12), the primary parameters of the 25 kV AC traction network were determined based on data from field experiments under short-circuit conditions. The calculations considered the following equipment: a TDTNZh-40000/110/27.5/10 traction transformer, a traction substation grounding grid with equivalent resistance up to 0.1 Ω, a transverse compensation unit with KS1-1.05-30 (13.5 μF) capacitors and 89.17 mH inductance, a PBSM1-95 + MF-100 catenary system, and R-65 rails.

The parameters were obtained using reference formulas and data from studies [8]-[15]. These values, corresponding to the equivalent circuit of the 25 kV traction network of the East Siberian Railway, were used in computer experiments to investigate short-circuit current characteristics. Based on equations (5)…(12) and the obtained parameters, a dedicated software package for modeling emergency and transient processes in the traction power supply system was implemented in the Delphi 7 environment.

The average spacing between traction substations

(TS) is approximately 40 km [16]. Since the traction network is typically fed from both ends, computations may be limited to half of the inter-substation section due to symmetry of electromagnetic effects.

The computer simulations were performed up to 20 km, i.e., to the midpoint of the inter-substation zone. The studies considered short circuits at distances of 1, 2, 3, 4, 5, 8, 12, 16, and 20 km from the TS under both summer and winter conditions. The rail-to-ground resistance values were assumed to be ($R_{r\text{-}G}$ = 0.25 Ω·km) for summer conditions and ($R_{r\text{-}G}$ = 25 Ω· km) for winter conditions [13], [17]-[21]. The results of the computer simulations are presented in Figures 5-11.

Figure 5 presents oscillograms of the TS voltage U_{TS} and the currents in the contact wire I_{CW} rails I_r, and ground I_G for a short-circuit phase angle ψ = 0º at a distance of 5 km under summer conditions. Approximately 49% of the short-circuit current returns through the ground. The contact wire current lags the TS voltage by φ = 56º.

Figure 6 depicts the corresponding waveforms under winter conditions with $R_{r\text{–}G}$ = 25 Ω·km at ψ = 0°. In this case, about 77% of the short-circuit current flows through the rails, and the phase lag increases to φ = 60°.

Simulation studies were also conducted to determine peak values of currents in the contact wire, rails, and ground at various short-circuit locations (1…20 km) for summer (Fig. 7) and winter (Fig. 8) conditions.

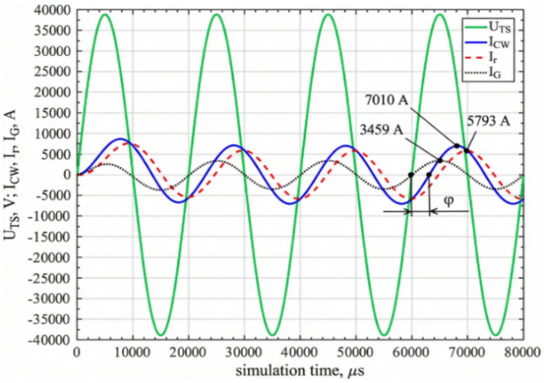

Figure 5: TS voltage and currents in the 25 kV AC traction network during a contact wire-to-rail short circuit at a distance of 5 km from the TS ($R_{r\text{-}G}$ = 0.25 Ω·km, summer conditions, ψ = 0º).

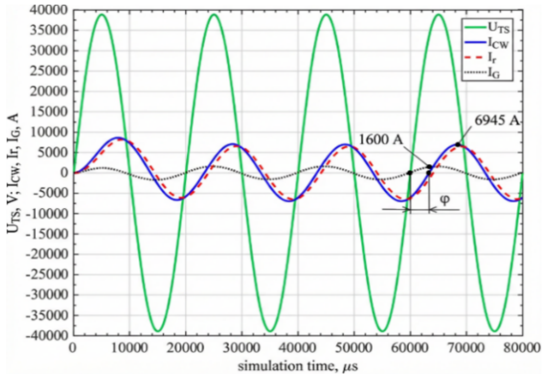

Figure 6: TS voltage and currents in the 25 kV AC traction network during a contact wire-to-rail short circuit at a distance of 5 km from the TS ($R_{r\text{-}G}$ = 25 Ω·km, winter conditions, ψ = 0º).

Table 1: Primary parameters of the equivalent circuit of the 25 kV AC traction network.

Simulation time, µs	80000	L_E, mH	7.514
Sampling interval, ns	2	R_E, Ω	0.113
Line length, km	20	R_{r1}, …, R_{r20}, Ω/km	0.11
Short-circuit voltage phase, rad	0 (1.57)	L_{r1}, …, L_{r20}, mH/km	0.803
U_{TS}, kV	38.89	R_{K1}, …, R_{K20}, Ω/km	0.085
R_L, Ω	5000	L_{K1}, …, L_{K20}, mH/km	0.904
C, µF	13.5	$R_{(r\text{-}G)1}$, …, $R_{(r\text{-}G)20}$, Ω·km (rail-to-ground)	0.25 – summer 25 – winter
L, mH	89.17	R_{G1}, …, R_{G20}, Ω·km	0.3
R_0, Ω	0.1	R_{Ir1}, …, R_{Ir20}, Ω/km	40000

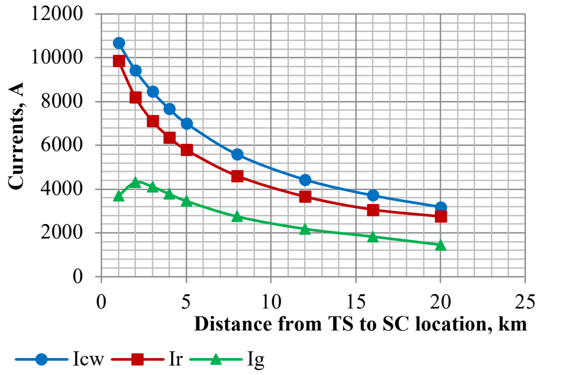

Figure 7: Peak currents in the contact wire (I_{CW}), rails (I_r), and ground (I_G) at the contact wire-to-rail short circuit location under summer conditions ($R_{r\text{-}G}$ = 0.25 Ω·km, ψ = 0°).

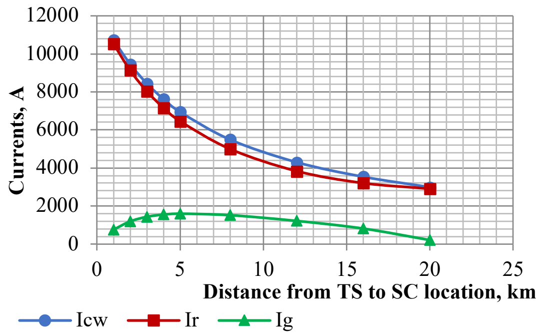

Figure 8: Peak currents in the contact wire (I_{CW}), rails (I_r), and ground (I_G) at the contact wire-to-rail short-circuit location under winter conditions ($R_{r\text{-}G}$ = 25 Ω·km, ψ = 0°).

The results show that under summer conditions the maximum ground current occurs within the first 10 km from the TS, whereas in winter the maximum is observed in the 4…8 km interval. The peak ground current in summer exceeds that in winter by a factor of 2.7.

Figure 9 shows the phase lag angles (φ) of the short-circuit current in the contact wire relative to the traction network supply voltage (U_{TS}). The increase in the angle φ under winter conditions can be explained by the enhanced influence of rail inductance due to higher short-circuit currents in the rails during winter.

Figure 10 shows the rail-to-ground voltage $U_{R\text{-}G}$ at a fault location 5 km from the TS. Under winter conditions, this voltage is eight times greater than under summer conditions and reaches 4839 V, exceeding the permissible insulation voltage U_{PERM} = 2.5 kV by a factor of two.

Figure 11 presents the amplitude values of $U_{r\text{-}G}$ at different fault distances. In summer, the voltage does not exceed permissible limits (U_{PERM} =2.5 kV), whereas in winter it surpasses allowable insulation levels along the entire section, necessitating protective measures against longitudinal overvoltages. Such overvoltages also pose a hazard to maintenance personnel.

Using the calculated phase relationships between the short-circuit current in the contact wire (I_{CW}) and the traction network supply voltage (U_{TS}) (Fig. 9), the short-circuit current amplitudes (Fig. 8), the voltage at the TS phase (U_M), and the half-wave duration of the traction current, it is proposed to represent the traction network under short-circuit conditions for the half-wave of the traction current by equivalent parameters, calculated using the following formulas:

$$R_{EQP} = (\cos\varphi \times U_M)/I_{CW}; \quad (13)$$

$$L_{EQP} = (\sin\varphi \times U_M \times \theta)/(I_{CW} \times \pi), \quad (14)$$

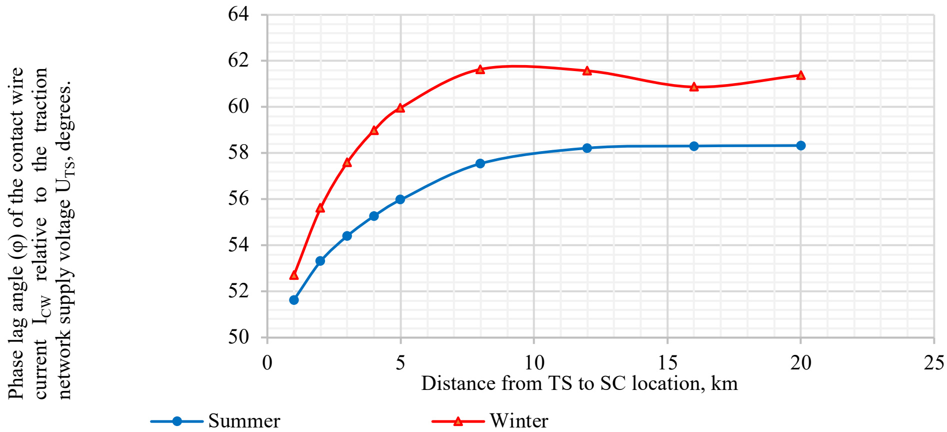

Figure 9: Phase relationship (φ) between the voltage at the TS and the current in the contact wire under summer. ($R_{r\text{-}G}$ = 0.25 Ω·km) and winter ($R_{r\text{-}G}$ = 25 Ω·km) conditions.

where R_{EQP} is the equivalent active resistance of the traction network for the short-circuit current in the contact wire; L_{EQP} is the equivalent inductance of the traction network for the short-circuit current in the contact wire; φ is the phase difference between the voltage and current in the contact wire; U_M is the amplitude of the voltage at the TS transformer, V; I_{CW} is the amplitude of the current at the short-circuit location, A; θ is the half-wave duration of the short-circuit current, s.

These expressions allow replacement of the complex traction network by equivalent resistance and inductance, simplifying the assessment of protective measures for railway automation and remote-control devices against switching overvoltages and overcurrents. Figure 12 shows the results of the calculations of equivalent parameters for a 25 kV AC traction network.

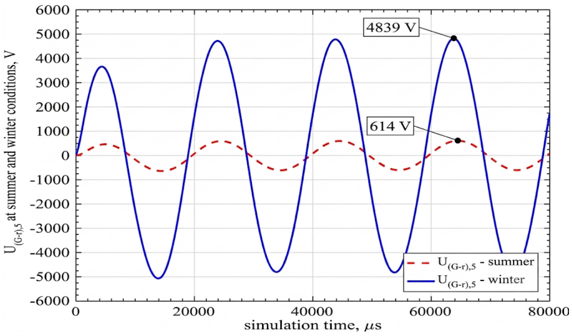

Figure 10: Voltage between the rail and ground $U_{(r\text{-}G)5}$ at the contact wire-to-rail short-circuit location 5 km from the TS under summer and winter conditions.

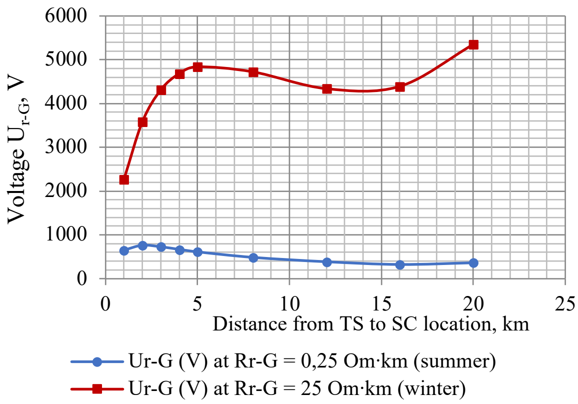

Figure 11: Amplitude values of the voltage between the rail and ground $U_{r\text{-}G}$ at the contact wire-to-rail short-circuit location under summer and winter conditions with ground resistance R_G = 0.3 Ω·km and ψ = 0°.

4 VERIFICATION OF THE MATHEMATICAL MODEL OF A 25 kV AC TRACTION NETWORK

The developed distributed-parameter model of the 25 kV AC traction network was validated by comparing simulation results with experimental data from an operational section [13].

The experimental baseline from [13] included measured short-circuit current amplitudes, rail-to-ground voltages, phase-shift data, and transient waveform characteristics obtained for operational traction-network conditions.

In the computational experiment, the parameters of the equivalent circuit from Table 1 were used. Validation considered multiple points along the inter-substation section (5, 10, 15, and 20 km from the traction substation) and analyzed peak short-circuit currents in the contact line I_{CW}^{max}, rail currents I_{r}^{max}, maximum rail-to-ground voltage U_{r-G}^{max}, phase shift φ, and transient waveform shapes. Engineering validation was based on relative errors of current and voltage amplitudes, phase deviation, and normalized root-mean-square error (NRMSE), since these metrics jointly characterize both the magnitude accuracy and the waveform similarity of transient responses.

Simulation results closely matched experimental data: current amplitude errors did not exceed 8%, voltage errors remained below 10%, phase deviations were within 5°, and waveform NRMSE values were mostly below 0.1 (see Table 3), confirming accurate transient reproduction. For instance, at 20 km from the traction substation under winter conditions, the simulated contact-wire short-circuit current was 1966 A at a phase angle of −56°, whereas the experimental value was 1820 A at −61°, corresponding to a 7.5% amplitude error and a 5° phase deviation. (see Table 2).

These results confirm that the model accurately reproduces transient processes across the inter-substation section and can be reliably used for the design of protection systems in railway automation and telemechanics against electromagnetic hazards.

4.1 Verification Conclusions

The obtained results confirm that the proposed model ensures high accuracy in both steady-state and transient conditions, making it suitable for the analysis and design of protection systems for railway automation under electromagnetic disturbances.

5 SCIENTIFIC NOVELTY

The scientific novelty of this study lies in the development of a distributed-parameter mathematical model of a 25 kV AC traction power network based on the state-variable method and a loop-branch topological matrix, which enables accurate simulation of transient electromagnetic processes under short-circuit conditions. A novel approach to assessing hazardous electromagnetic interference (HEMI) affecting railway track circuit equipment is proposed by jointly considering fault location, seasonal variations in rail-to-ground resistance, and the dynamic distribution of return traction currents. The study establishes quantitative relationships between short-circuit current distribution, rail-to-ground overvoltages, and environmental operating conditions, demonstrating that under winter conditions the resulting overvoltages may exceed the permissible insulation limits of track circuits by more than twofold.

Another contribution is the introduction of an equivalent representation of the traction network during fault conditions using generalized resistance and inductance parameters for each half-cycle of the short-circuit current, thereby simplifying engineering assessment of electromagnetic impacts on railway automation systems. A method for determining these equivalent parameters from the amplitude-phase characteristics of currents and voltages is also developed, allowing the transformation of a distributed mathematical model into an engineering-oriented equivalent circuit suitable for practical applications. The adequacy of the proposed model is confirmed through comparison with field experimental data, yielding deviations below 8%, which demonstrates its suitability for the design and analysis of railway protection systems. Overall, the study advances electromagnetic compatibility modeling by integrating distributed traction network parameters and transient electromagnetic processes within a unified computational framework.

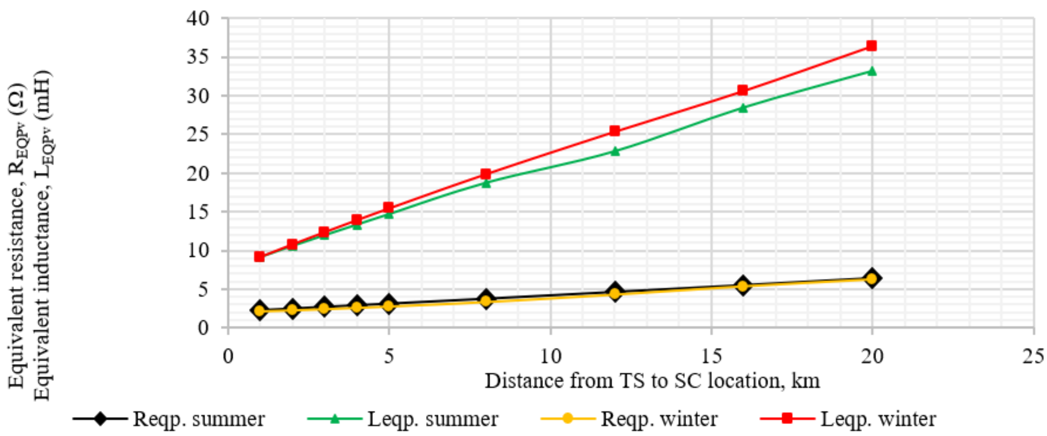

Figure 12: Equivalent parameters of the traction network.

Table 2: Comparison of Simulation and experimental results for hort-circuit conditions.

Distance from TS, km	Parameter	Simulation	Experiment	Absolute Error	Relative Error, %
5	I_{CW}^{max}, A	3120	2950	170	5.8
	U_{r-G}^{max}, V	2100	1950	150	7.7
	(φ), deg	54	57	3	5.3
10	I_{CW}^{max}, A	2750	2600	150	5.7
	U_{r-G}^{max}, V	3200	3000	200	6.7
	(φ), deg	55	59	4	6.8
15	I_{CW}^{max}, A	2300	2150	150	7.0
	U_{r-G}^{max}, V	4100	3800	300	7.9
	(φ), deg	56	60	4	6.7
20	I_{CW}^{max}, A	1966	1820	146	7.5
	U_{r-G}^{max}, V	4839	4500	339	7.5
	(φ), deg	56	61	5	8.2

Table 3: NRMSE-based comparison of simulated and experimental waveforms.

Distance from TS, km	Signal	NRMSE	Max Deviation	Interpretation
5	$I_{CW}(t)$	0.082	6.5%	High accuracy
	$U_{r-G}(t)$	0.095	7.2%	High accuracy
10	$I_{CW}(t)$	0.076	6.0%	High accuracy
	$U_{r-G}(t)$	0.088	6.8%	High accuracy
15	$I_{CW}(t)$	0.089	7.1%	High accuracy
	$U_{r-G}(t)$	0.097	7.5%	High accuracy
20	$I_{CW}(t)$	0.094	7.8%	High accuracy
	$U_{r-G}(t)$	0.102	8.1%	Acceptable accuracy

6 CONCLUSIONS

A distributed-parameter model of a 25 kV AC traction network as a source of HEMI affecting railway automation and remote-control devices was developed. Transient processes during contact wire-to-rail short-circuits were analyzed with respect to distance from the short-circuit to the traction substation, network parameters, and rail-to-ground insulation under summer and winter conditions.

During summer, the voltage remains within the permissible limit (U_{PERM} = 2.5 kV), while in winter it exceeds allowable insulation levels along the entire section, requiring protective measures against longitudinal overvoltages. These overvoltages also present a safety risk to maintenance personnel.

The model simplifies complex electromagnetic interactions by using equivalent parameters (equivalent inductance and resistance) for each half-wave of the short-circuit current, facilitating the analysis of protective measures for automation and control devices against overcurrents and switching overvoltages.

Application of the model allows: determination of limiting characteristics of choke- and railway transformers considering magnetic coupling and core saturation effects, and justification of protective measures to limit energy on protection devices before core saturation. The results support the design of coordinated cascaded protection systems, combining functional (transformers and choke-transformers) and supplementary (overvoltage/overcurrent) protection against HEMI.

REFERENCES

[1] A. Manakov and A. Rakhmonberdiev, “Dangerous electromagnetic impact of the reverse traction network of 25 kV AC on railway automation devices,” Automation in Transport, vol. 8, no. 3, pp. 233-251, 2022, [Online]. Available: https://doi.org/10.20295/2412-9186-2022-8-03-233-251.

[2] E. Chakhmakhsazyan, Yu. Barmakov, and A. Goldenberg, Machine Analysis of Integrated Circuits: Theory and Programming Issues. Moscow, USSR: Soviet Radio, 1974.

[3] E. Kuh and R. Rohrer, “The state-variable approach to network analysis,” in Proceedings of the IEEE, vol. 53, no. 7, pp. 672-686, Jul. 1965, [Online]. Available: https://doi.org/10.1109/PROC.1965.3991.

[4] V. Zakaryukin, A. Kryukov, and E. Alekseenko, “Modeling of emergency operating modes in AC railway traction networks,” iPolytech Journal, vol. 21, no. 3, no. 122, pp. 100-109, 2017.

[5] A. Manakov and A. Rakhmonberdiev, “System for protecting rail circuit equipment from emergency processes in the AC traction network,” AIP Conference Proceedings, vol. 3331, no. 1, 2025, [Online]. Available: https://doi.org/10.1063/5.0307074.

[6] K. Chao, “State-Variable Techniques,” in Circuit Analysis and Feedback Amplifier Theory, W.-K. Chen, Ed. Boca Raton, FL, USA: CRC Press, 2005.

[7] V. Yagup and E. Yagup, “Analysis of the operating mode of an electric power network using the state variable method,” East European Journal of Advanced Technologies, no. 1/6 (43), pp. 43-46, 2010.

[8] Yu. Bey, R. Mamoshin, V. Pupynin, and M. Shalimov, Traction Substations. Moscow, USSR: Transport, 1986.

[9] A. Azizov, S. Ubaydullayev, and E. Ametova, “Model of push-button relay circuits for shunting routes,” AIP Conf. Proc., vol. 2612, p. 060020, Mar. 2023, [Online]. Available: https://doi.org/10.1063/5.0116123.

[10] A. V. Kotelnikov, A. V. Naumov, and L. P. Slobodanyuk, Rail Circuits under the Influence of Grounding Devices. Moscow, USSR: Transport, 1990.

[11] A. Azizov and E. Ametova, “General principles of application of temporal Petri nets in intelligent real-time decision support systems of railway automation of Uzbekistan,” in Proc. Int. Conf. Applied Innovation in IT, 2025, [Online]. Available: https://doi.org/10.25673/120438.

[12] B. Borodulin, Capacitor Units of Electrified Railways. Moscow, USSR: Transport, 1983.

[13] R. Karyakin, AC Traction Networks, 2nd ed. Moscow, USSR: Transport, 1987.

[14] V. Havryliuk, "Modelling of the Return Traction Current Harmonics Distribution in Rails for AC Electric Railway System," in IEEE 2018 International Symposium on Electromagnetic Compatibility, Aug. 27-30, 2018, [Online]. Available: https://doi.org/10.1109/EMCEUROPE.2018.8485160.

[15] X. Guo, Q. Li, S. Xie, and H. Wang, "Modeling and capacitance effect analysis of the cable traction network of an electrified railway," Proc. IMechE Part F: J. Rail and Rapid Transit, Jul. 15, 2015, [Online]. Available: https://doi.org/10.1177/0954409715615157.

[16] R. Miroshnichenko, Operating Modes of Electrified Sections. Moscow, USSR: Transport, 1982.

[17] E. Ametova, "Framework development for software functionality in Uzbekistan's block route centralization system," E3S Web of Conferences, 2024, [Online]. Available: https://doi.org/10.1051/e3sconf/202459207017.

[18] N. Aripov, O. Kadirov, and A. Sadikov, "Dispersion approach to solving the problem of statistical linearization for nonlinear identification of signals," AIP Conf. Proc., vol. 3331, no. 1, p. 040011, Nov. 2025, [Online]. Available: https://doi.org/10.1063/5.0307057.

[19] A. Azizov, E. Ametova, Q. Nuriddinov, and S. Ubaydullayev, "The operation model of the point setting relay for a microelectronic device," E3S Web of Conferences, vol. 515, p. 04001, 2024, [Online]. Available: https://doi.org/10.1051/e3sconf/202451504001.

[20] Z. Yusupov, A. Azizov, E. Ametova, and S. Ubaydullaev, "Model of circuits of anti-repeat relays of train routes," Lecture Notes in Networks and Systems, vol. 718, 2024, [Online]. Available: https://doi.org/10.1007/978-3-031-51521-7_21.

[21] N. Yaronova, E. Khidirov, and J. Kurbanov, "Duties and obligations of the railway staff concerned when the microprocessorized contactless controlling gauge device signal is triggered," Lecture Notes in Electrical Engineering, vol. 1324, 2025, [Online]. Available: https://doi.org/10.1007/978-3-031-82494-4_6.